Stick–slip behavior of serrated flow during inhomogeneous deformation of bulk metallic glasses

Florian H. Dalla Torre [*], David Klaumünzer, Robert Maaß, Jörg F. Löffler

Laboratory of Metal Physics and Technology, Department of Materials, ETH Zurich, Wolfgang-Pauli-Strasse 10, 8093 Zurich, Switzerland

Abstract

Accurate compression tests with a piezoelectric load cell and an acquisition rate of up to 10 kHz were performed on a Zr-based bulk metallic glass in the temperature range 210–320 K at a strain rate of 10^{-3} s^{-1}. Information about the stress drop magnitude and the associated size of shear displacements as a function of temperature and strain provides detailed insights into the shear band characteristics, which can be described by a stick–slip process. The average shear slip displacement is on average about 1–2 μm, irrespective of temperature, whereas the associated slip time (or stress drop time) increases from ∼1 ms at 320 K to ∼0.4 s at 213 K, yielding values on the deformation kinetics and the shear viscosity. Scanning electron microscopy investigations on shear surfaces and in situ acoustic emission measurements provide further understanding into the complex multistep shear slip process.
© 2010 Acta Materialia Inc. Published by Elsevier Ltd. All rights reserved.

1. Introduction

At ambient temperature plastic deformation in most bulk metallic glasses (BMGs) proceeds in a jerky and spatially inhomogeneous manner confined to thin shear bands. Similarly, confined jerky deformation occurs also in various other materials and circumstances as, for instance, in boundary lubrication problems, where two solids slide along each other producing stick–slip motion [1,2], or in seismically active geological faults, which can be described using stick–slip models, with earthquakes being generated during periods of rapid slip [3,4]. Polycrystalline alloys can also exhibit such jerky inhomogeneous deformation, the most prominent examples of which are related to the Portevin–Le Châtelier effect [5,6]. Experimentally, such behavior is typically reflected in serrated flow curves, where under compressive loading at constant strain rate, stress drops emerge, which in cases of macroscopic BMGs have

magnitudes of the order of a few tens of MPa [7–12]. The origin of such stress drops may be explained by the nature of shear banding in which discrete plastic shear events are activated simultaneously, reaching several orders of magnitude faster local strain rates than the applied machine strain rate during the subsequent elastic loading. Micromechanically, one can imagine that the simultaneous nucleation of multiple atomic shear events triggers the generation and propagation of shear bands, resulting in displacement bursts of a few hundred nanometers to a few micrometers in BMGs of standard sample dimensions [13,14]. This shear-induced softening and the consequent decrease in viscosity during a stress drop is in the literature classically either related to a temperature burst or to shear dilatation, i.e. free volume generation phenomena, and will be discussed in more detail below (see also Refs. [15,16] and references therein).

For BMGs there is still uncertainty surrounding the temperature rise within a shear band during inhomogeneous flow. Lewandowsky and Greer demonstrated with a fusible coating technique that temperatures significantly higher than the melting point of tin (232 °C) are locally

---

[*] Corresponding author.

E-mail addresses: florian.dallatorre@mat.ethz.ch, florian.dallatorre@swissmetal.com (F.H. Dalla Torre).

present during shear banding [15]. Subsequent further detailed work by these authors indicated that in bending experiments local melting of tin only occurred at shear offsets larger than about 1 μm. Meanwhile it is not clear if local melting is associated with shear banding with or without fracture [17]. In contrast, high-speed thermographic and spectroscopic measurements have been applied to capture temperature rises during shear banding and fracture [18–23]. Despite the different experimental techniques used and the diverse theoretical approaches taken to deduce a temperature estimate within shear bands—including adiabatic and non-adiabatic conditions [15,17–26]—it is clear that shear bands exhibit temperatures of several hundred degrees at final fracture. However, more diverse opinions exist for shear banding before fracture and whether heating is regarded as a critical factor in, or a consequence of, shearing [15,27–29]. These difficulties in measuring and theoretically approximating the temperatures within shear bands of metallic glasses are closely related to the extreme spatial and temporal localization of shear banding, which is much more pronounced than in any other type of solid material. Transmission electron microscopy (TEM) has revealed shear band widths of a few tens of nanometers [30–32], while atomic size shear events occurring within time intervals of the order of nanoseconds [15] may only subsequently (by a poorly understood autocatalytic process) evolve into microscopic shear bands. Recent high-resolution scanning electron microscopy images show that river and other flow patterns are also present before fracture, but that their lateral thickness is roughly 10 times smaller than the flow layer in a shear band at fracture [13]. This agrees with the work reported in Refs. [33,34]. Thus, if one regards a temperature rise as the major cause of a change in viscosity, temperatures close to or above the glass transition temperature can in fact be expected during shear banding even before fracture. In disagreement with models suggesting a thermal spike, the time periods associated with micrometer-sized strain bursts are of the order of a few milliseconds, in agreement with the current literature [35,29,36]. As also pointed out in Refs. [35,29], these time periods are far too long to keep temperatures within shear bands high enough to cause a significant drop in viscosity during room temperature (RT) testing. Thus, temperature per se may not be the main cause of the large drop in viscosity at RT. Alternatively shear-induced dilatation or shear softening via free volume generation as proposed by Spaepen [37–39] provide a plausible explanation for the experimental observations. As will be shown, we extend the observations of Refs. [35,29,36] to a larger temperature range within the inhomogeneous flow regime. This powerful method of discriminating discrete shear band bursts provides estimates of the shear strain rates and its associated viscosity during inhomogeneous micrometer-scale shear displacements, and thus gives information about the underlying shear band mechanism. In order to shed light on the question of shear band nucleation and its propagation, we present in the second part of this paper the results of acoustic emission (AE) measurements performed in situ during compression testing. Due to the high sensitivity of the AE signals towards minute, collective displacements in solids, and due to the very high acquisition rate (MHz), a more refined characterization of the shear band process is possible.

2. Experimental

A master alloy of composition $Zr_{52.5}Cu_{17.9}Ni_{14.6}Al_{10}Ti_5$ (Vit105) was produced by arc melting in an inert argon atmosphere (99.9999% purity) and subsequent suction casting into rods 3 mm in diameter. Compression test specimens 5 mm in length were cut from these rods and the compression planes were polished to ensure parallel alignment. Compression tests were performed on a screw-driven Schenck–Trebel machine equipped with a 100 kN load cell. In addition, a piezoelectric 60 kN load cell (Kistler) was mounted in direct proximity to the specimen in order to shorten the elastic wave propagation time from the specimen to the load cell; moreover, piezoelectric load cells have a faster and more accurate response compared to conventional 100 kN load cells. Fig. 1 shows a detailed view of a load–time curve recorded during compression testing of a silicon (Si) sample exhibiting brittle fracture. As can be seen, the load drop caused by microcracking of the specimen occurs within a fraction of a millisecond (∼0.2 ms), which can be taken as the lower limit of the load cell response time for a material fracturing at the speed of sound. The delayed response time (∼0.4 ms) of the conventional load cell can be explained by the time the elastic wave needs to reach from the sample position to the load cell (0.5 m). Strain was measured from the cross-head displacement as well as by a 20 mm clip gauge bridging the upper and lower compression
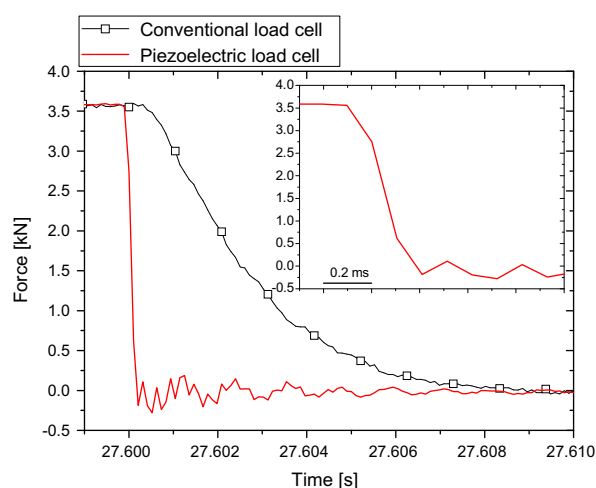

Fig. 1. Enlarged section of a force–time curve of a compressed silicon sample recorded with the piezoelectric 60 kN (thick red) and conventional 100 kN load cell (thin black line with square symbol). The piezoelectric load cell yields a response time of only ∼0.2–0.3 ms, while a response time of ∼10 ms is measured with the conventional load cell (For interpretation of the references to colour in this figure legend, the reader is referred to the web version of this article.).

platens. The data was acquired using an analog/digital converter with an acquisition rate of up to 10 kHz and moving average filtering over eight consecutive points. AE signals were recorded with an commercial AE setup (AMSY-5, Vallen System GmbH) using an acquisition rate of 2 MHz. Both resonant frequency (250 kHz) and broad-band AE sensors (frequency range 20–1000 kHz) were attached to the compression plates. Cross-head velocities of 0.6–0.01 mm min^{-1}, equating to strain rates of 2×10^{-3} and 3×10^{-5} s^{-1}, respectively, were used. Experiments were conducted at different temperatures between 323 and 77 K by using a climate chamber or by immersing the samples in different cooling mixtures [40]. The temperature was kept constant within a range of ±3 K.

3. Results

3.1. Temperature dependence of serrated flow

The temperature dependence of serrated flow reveals a clear increase in the serration stress amplitude with increasing temperature (in particular near the transition temperature; see Fig. 2). For temperatures higher than 325 K, the samples show no plastic strain due to elevated temperature embrittlement [40]. At RT and up to 325 K, stress drops of 20 MPa are typical, while at 200 K the serrations are almost absent. This temperature corresponds to the transition temperature between serrated and non-serrated flow as the strain rate increases from 1×10^{-5} to 1×10^{-4} s^{-1} in Vit105 [14,40]. Fig. 3 shows a detailed view of the serrated and non-serrated stress–strain curve at 200 K, demonstrating evidence of increased resistance to flow for the serrated part at a strain rate of 1×10^{-5} s^{-1}. At the higher strain rate, smooth, continuous yielding occurs at a lower plastic flow stress than that required for activating plastic shear during serrated flow. At the lower strain rate, part of the stored elastic energy is dissipated by discrete and sudden stress drops, causing shear offsets of up to a few micrometers in size (see also Fig. 4). The magnitude of the shear dis-
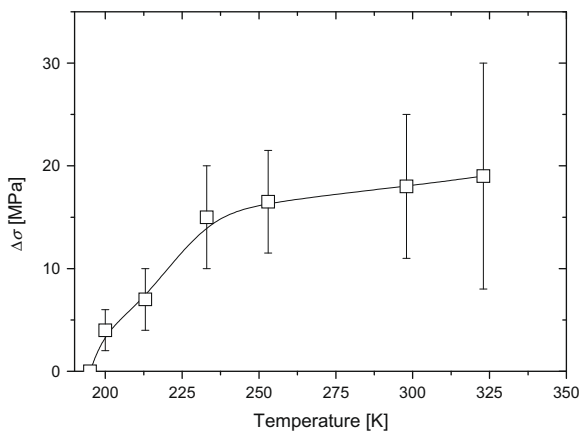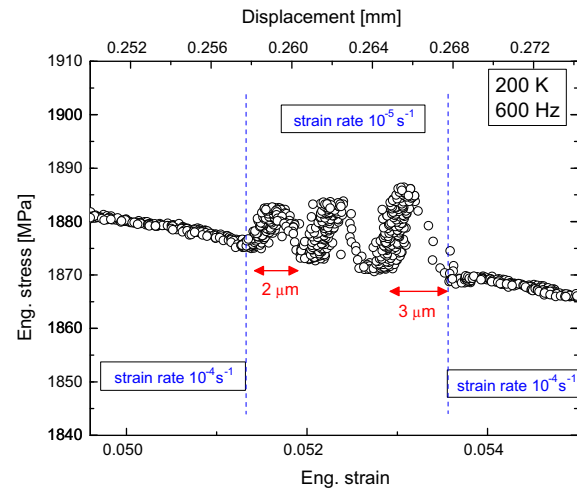

Fig. 3. Engineering stress–strain (displacement) curve showing the transition from non-serrated to serrated flow at 200 K when decreasing the strain rate by one order of magnitude from 10^{-4} to 10^{-5} s^{-1}.

placement varies with stress drop amplitude from a few hundred nanometers to a few micrometers of displacement, in agreement with observations made by Refs. [33,41]. In fact, with increasing compressive strain the stress drop amplitude increases [11], while the associated stress drop time decreases, as shown in Fig. 4a for a test performed at −30 °C. Just after yielding, the stress drop magnitude is a few MPa and increases to 80 MPa before fracture—an almost 10-fold increase. The datapoint at 1890 MPa indicates the fracture of the specimen. It should be noted that the magnitude of the stress drops is not only a material property, but is dependent on the stiffness of the apparatus [10]. Fig. 4b correlates the measured values for Δt to the shear displacement bursts for a single test conducted at −30 °C. The majority of all strain bursts are within 1–2 μm, irrespective of the associated time Δt. Only in the last part of deformation does the strain burst magnitude increase to about 4–5 μm. Thus, as also mentioned in Ref. [11], the stress drop velocity increases with increasing strain. In analogy, but much less pronounced, an increase in shear velocity with increasing strain is observed. Interestingly, the onset of the increase in the serration strain coincides with the decrease in the flow stress level (for more details on shear band velocity, see Ref. [42]). These observations can be taken as indication of a multiple reactivation of the same shear zone memorizing its strain history. Applying the concept of the free volume model to this experimental evidence suggests that the reactivation of the same shear band will lead to a gradual increase in free volume, i.e. to shear softening.

The SEM images in Fig. 5 taken from different specimens tested at −150 °C (Fig. 5a) and at −20 °C (serrated flow) (Fig. 5b and c) show the surfaces of the major shear bands running through the sample. In order to examine these shear planes the compression tests were stopped before failure of the samples occurred. In Fig. 5a, shear striations run along the shear plane in the direction of
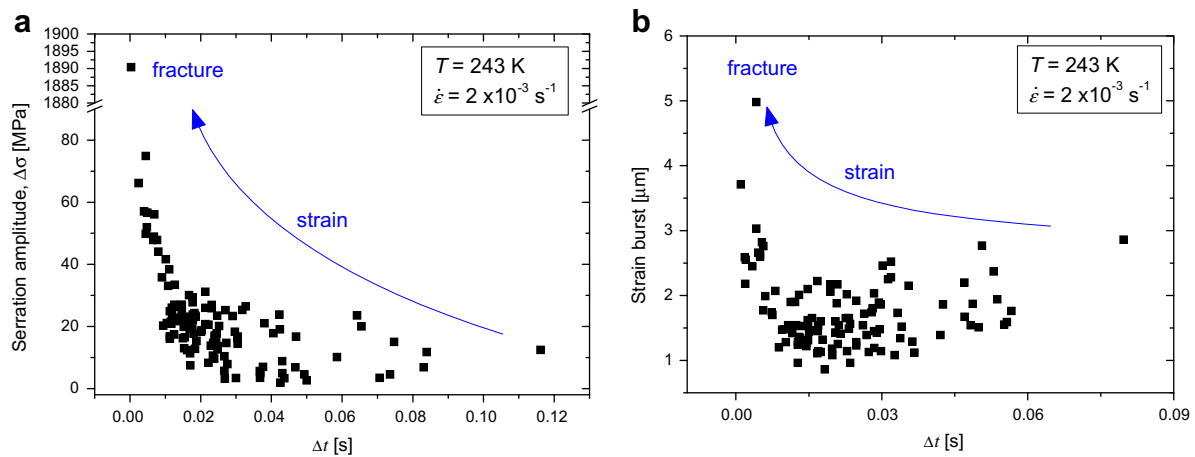

Fig. 2. Stress drop magnitude vs. applied temperature; the stress drop magnitude is averaged over a strain interval ranging from 0.04 to 0.06.

Fig. 4. Typical behavior of (a) stress drop amplitude (serration amplitude) and (b) shear burst displacement vs. shear event duration (Δt) extracted from a compression test performed at 243 K. Note that the serration amplitude increases with increasing strain and decreasing Δt.

shear, and are interrupted by vertically aligned shear steps of varying size and spacings from several hundred nanometers to a few micrometers. On the right-hand side of Fig. 5a there are indications of viscous flow lines. In Fig. 5b and c more detailed views of successions of shear striations separated by shear steps are shown. Fig. 5b shows shear steps of similar spacing as in Fig. 5a and c, but due to their lateral position on the shear plane, they lie at an oblique angle to the shear striations. As the spacing between the shear steps is of similar size to the strain bursts measured by the clip gauge, it is plausible to assume that a single major shear event is associated with a single stress drop [13,33]. In addition, it is worth mentioning that this structure is similar to shear planes found in rock-forming minerals [43,44] and suggests a typical stick–slip behavior as also seen in the stress–strain curve. In terms of step size, no clear difference was found for the samples tested at the two different temperatures. This qualitative observation agrees well with finding that the displacement bursts measured for each test are independent of temperature. Fig. 6 shows that the mean strain bursts remain constant with increasing temperature, with mean values of the order of 1.2–1.6 µm.

Fig. 7 shows the time associated with a single stress drop as a function of the applied temperature. Here the data are presented in logarithmic scale for the stress drop time Δt vs. the inverse of the applied temperature (Arrhenius plot). Since the influence of strain rate on Δt is negligible, data from strain rates of 10^{-3}–10^{-4} s^{-1} are summarized. In this log Δt vs. $1/T$ representation the duration of a shear event
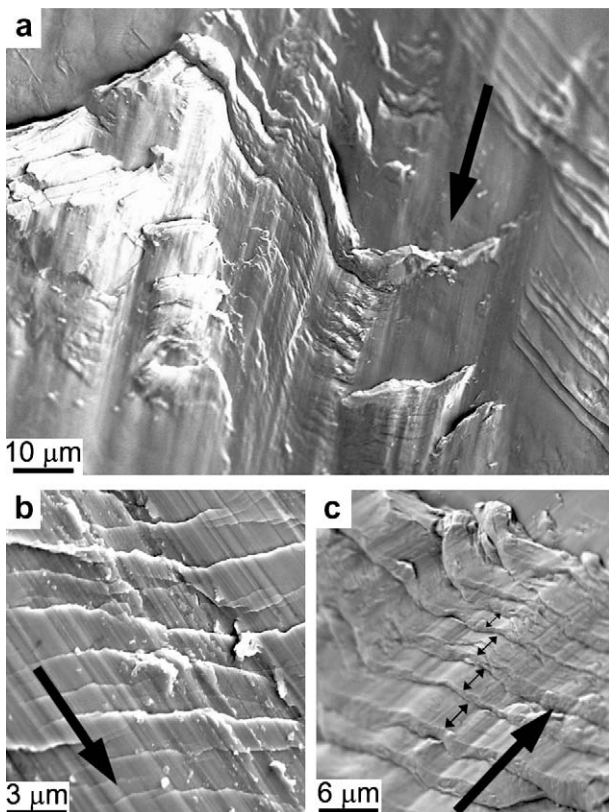

Fig. 5. SEM images of shear surfaces of non-fractured samples (a) tested at 123 K (non-serrated regime) and (b and c) tested at 253 K (serrated regime).
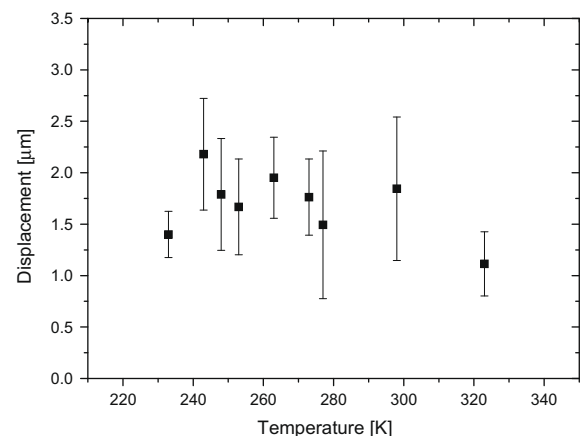

Fig. 6. Shear burst displacement vs. temperature for intermediate strain ranges.
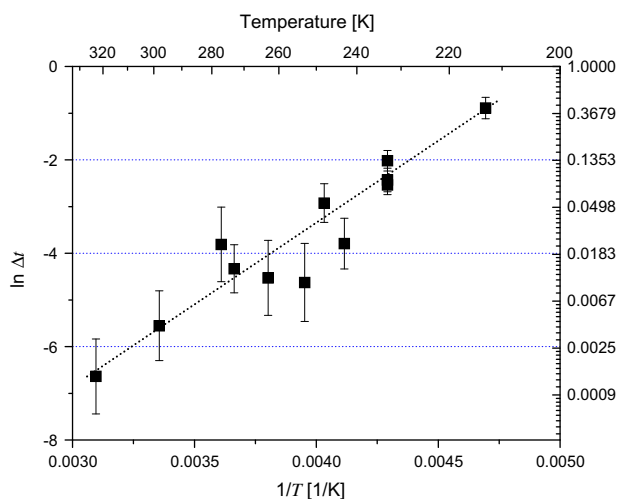
Fig. 7. Arrhenius plot of stress drop duration (Δt) vs. applied temperature.
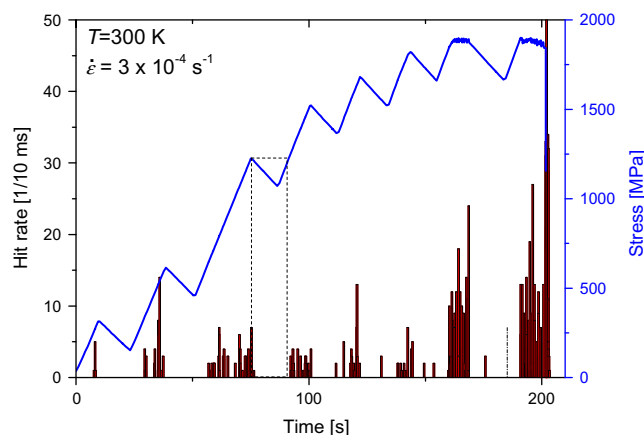

Fig. 8. Acoustic emission hit rate and compression stress measured as a function of time during a repeated loading and unloading experiment. The absence of AE signals until reaching a new maximum stress level provides evidence for the presence of the Kaiser effect in Zr-based BMG.

increases linearly with decreasing temperature, indicating that the deformation kinetics is strongly temperature dependent (for more details see Ref. [42]). Assuming that the duration of a stress drop is indicative of the duration of the deformation process, it can be directly related to the time taken by a shear band to become activated, slip and get arrested. In this case the measurements conducted reflect the temperature and strain rate dependence of the shear band velocity in Vit105 and the shear viscosity associated with shear banding can be estimated as shown in Section 4.

3.2. Acoustic emission measurements

In situ AE testing provides a powerful method to gain further insight into the characterization of the shear-banding process in metallic glasses. As mentioned in Section 1, a definitive method for evaluating the characteristic parameters of shear band nucleation and propagation and the possible associated local temperature bursts is still missing [13,15,18–22,26,27,31,33–35]. In this regard AE measurements may represent a potent alternative method because of their extremely high sensitivity with regards to the detection of elastic wave propagation by small-scale structural rearrangements and the high acquisition rates possible. As shown in the cyclic compressive loading–unloding curve (Fig. 8), AE signals appear in the elastic flow regime only once the previously reached maxima of the applied stress have been exceeded. This phenomenon, the so-called "Kaiser effect", is well known for crystalline metals and has also been noted in metallic glasses [45,46]. While in crystalline alloys it is regarded as being due to screening or activation of low-energy dislocation structures with subsequent strain hardening, in metallic glasses its origin may be attributed to an irreversible activation of highly localized plastic deformation, either at sites of internal stress concentration or low activation energy with respect to accommodating

plastic strain, as apparent from the framework of the potential energy landscape model [47] and the associated relaxation phenomena [48,49]. In addition, it can be seen from Fig. 8 that the AE amplitude increases towards the transition to the plastic regime.

Fig. 9a and b show magnified views of a stress–strain curve with the characteristic serrated flow behavior recorded at RT, demonstrating that the AE bursts correlate with the onset of the stress drops and that the stress drop magnitude is not correlated with the amplitude of the AE signal (Fig. 9b). Fig. 9c and d show the recorded AE signal for a typical AE burst (wavelet). Some distinctive features are worth noting. Preceding a sharp rise in AE amplitude, two small events can be detected (precursors). The main AE signal shows a region of constantly high amplitude extending over less than 1 ms. Continuous attenuation of the signal then follows, leading to a typical tail which is generally attributed to resonances within the sensor. Fig. 9d is a close-up view of the initially high amplitude part of the signal shown in Fig. 9c. It can be clearly seen that multiple discrete AE bursts of rise times of approximately 0.1 ms are present, in agreement with results of Vinogradov et al. [46]. Most importantly, the duration of this high-amplitude region (~0.5 ms) is shorter than the stress drop duration at RT (1–6 ms, Fig. 7). These results give a clear fingerprint of the shear banding characteristics, and will be discussed further in Section 4.

4. Discussion

4.1. Shear strain rate and apparent viscosity

The flow patterns on fracture surfaces are indicative of a rheological change in the structure at fracture, which is characterized by a drastic drop in viscosity. In analogy, Fig. 10 shows liquid-like structures on a non-fractured sample deformed at −150 °C (non-serrated flow regime) indicative of a drop in viscosity during shear banding. Sim-
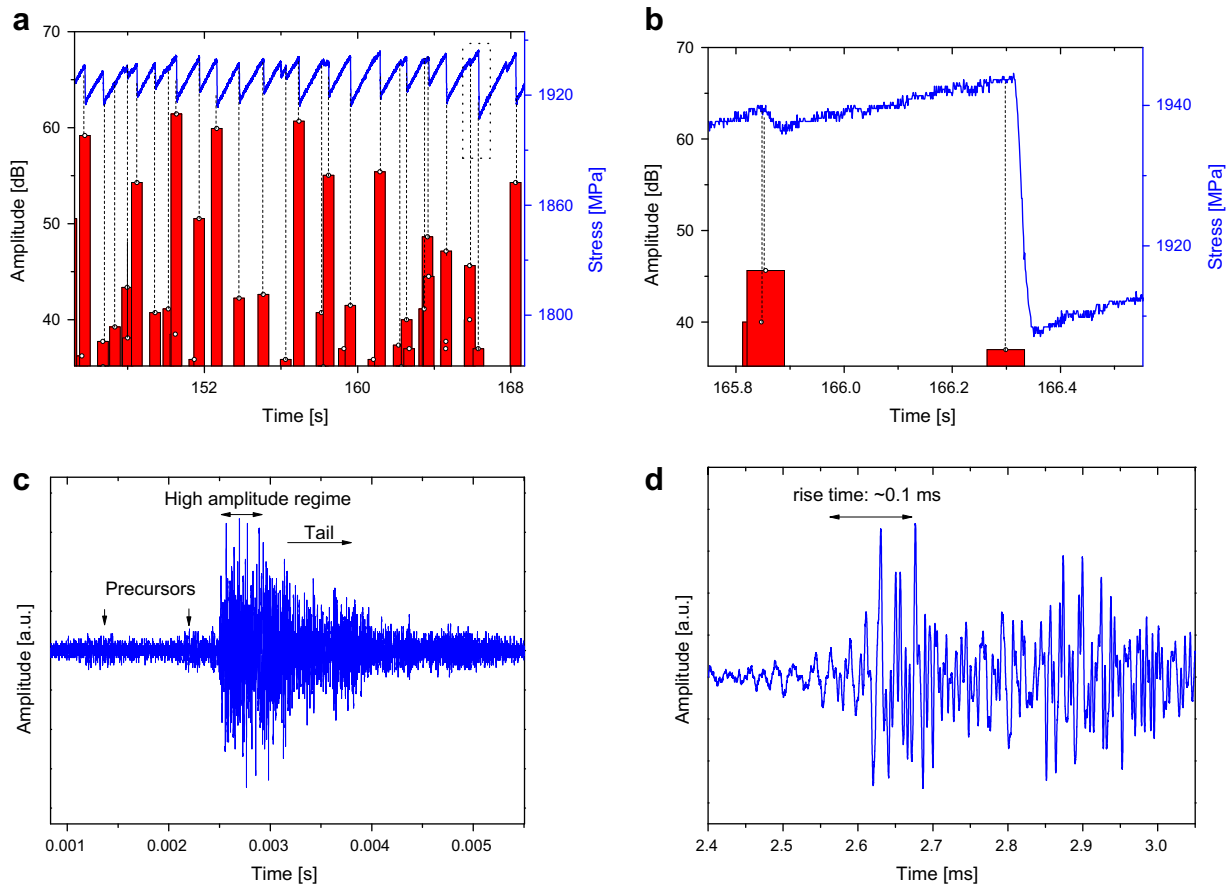
Fig. 9. Acoustic emission amplitude measured in situ during a compression test performed at room temperature. (a and b) Details on the variation of acoustic emission amplitude in relation to the magnitude and presence of serrations. (c and d) Typical waveforms corresponding to signals recorded during these discrete shear events.

ilar observations have been made on non-fractured samples deformed at RT [13,33]. From these observations we can confirm the general concept of deformation models in which sudden viscosity drops are inherent to localized deformation, and prove that they also occur in deformed
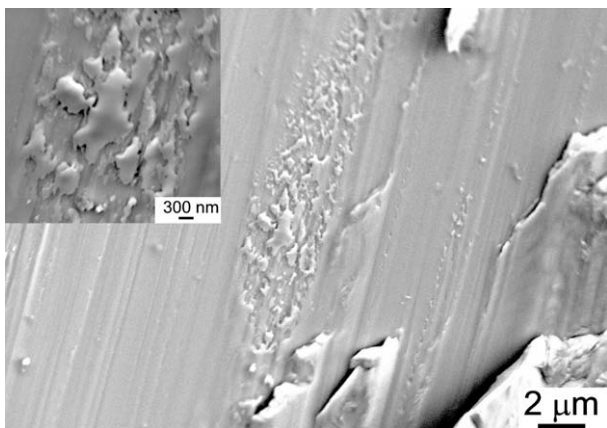

Fig. 10. Shear surfaces of a non-fractured compression test specimen deformed at a temperature of 123 K (within the non-serrated regime). As well as parallel shear striations and shear steps, liquid-like smeared droplets are visible (see inset).

samples prior to fracture even at very low applied temperatures. During a compression test the single shear bursts (shear displacement) increase markedly in magnitude as the associated time is reduced, reaching maximum displacements and shear strain rate prior to failure (Fig. 4). This is indicative of strain softening due to the reactivation of the same shear zone. Whether the maximum shear strain rate measured just before failure corresponds to an intrinsic maximum strain rate which the sample can sustain is currently under investigation.

The SEM studies on non-fractured samples presented here (Fig. 5) and in our earlier work [13] clearly indicate that shear does not occur on one single plane, but is rather localized to a shear zone with numerous shear planes stacked on top of each other, extending over a few hundred nanometers to a few micrometers (for serrated and non-serrated regimes). Fig. 11 shows a schematic view and SEM image of a deformed but not fractured compression test sample with a major shear zone highlighting the typical shear steps. The SEM image shows the front view of shear steps at the outer edge of the sample. In consideration of the above-mentioned points, the presented view favors a simultaneous shear model, where the velocity within each shear band is directly related to the shear displacement
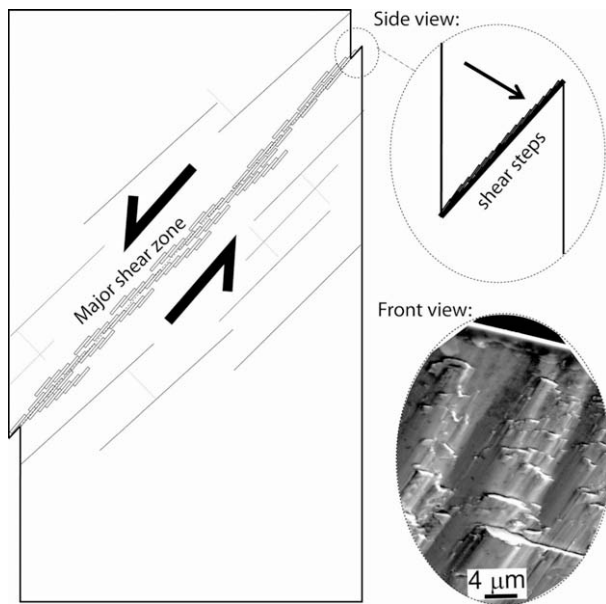
Fig. 11. Schematic image of a deformed specimen indicating a major shear zone with shear steps that comprise multiple parallel shear bands. Front view SEM image of the edge of a shear plane showing shear steps indicating multiple shear bands.

yielding a local shear strain rate $\dot{\gamma}$. According to the relation $\eta_{shear} = \tau/\dot{\gamma}$, an apparent shear viscosity can be derived, where the shear stress τ is calculated from the macroscopic flow stress σ_{flow} by $\tau = \sigma_{flow}/2.01$, and the shear strain rate is calculated from $\dot{\gamma} = \Delta w/(x\Delta t)$, where Δw is the shear displacement, x is the thickness of a shear band and Δt is the time required for the event to occur. Assuming that shear occurs simultaneously on a number, N, of parallel planes within a shear zone, however, leads to a lower effective shear strain rate per shear band, as defined by $\dot{\gamma} = \frac{\Delta w}{Nx\Delta t}$. In Ref. [13] a value of $\sim$0.5 μm was estimated for Nx, so N would be equal to 25–50. Using an average value of 1.6 ± 1.0 μm for the shear displacement burst Δw (in agreement with previous works for RT testing [13,33,34,27]) together with a value of 0.4 s for Δt, as measured at 200 K, yields an average shear strain rate of $\dot{\gamma}$ $\sim$200 s^{-1} for $Nx = 20$ nm (corresponding to a single shear band) and 8 s^{-1} for $Nx = 500$ nm (corresponding to a shear zone). These values increase with increasing temperature, and at 323 K ($\Delta t \sim$0.001 s) the upper boundary for $\dot{\gamma}$ is estimated to be of the order of $\dot{\gamma} \sim$80,000 s^{-1} for $Nx = 20$ nm and $\dot{\gamma} \sim$3200 s^{-1} for $Nx = 500$ nm.

Fig. 12a shows the apparent shear viscosity as a function of the externally applied temperature for $Nx = 20$ nm and $Nx = 500$ nm, indicating a decrease in viscosity with increasing temperature. Similar values have recently been published in Ref. [35] for tests performed at RT. Interestingly, the viscosities in the serrated flow regime are within the range of viscosities measured in similar alloys at temperatures close to and above the glass transition temperature, T_g [50–52]. Thus, a viscosity change from 10^7 to 10^5 Pa s as measured here in the inhomogeneous flow regime would correspond to a temperature difference of only 30–50 K in the homogeneous deformation regime (e.g. Fig. 5 in Ref. [51]). This agrees well with the fact that the microstructural viscous flow features found on shear surfaces at RT and at 77 K are remarkably similar [14]. Despite the significant differences of the stress drop amplitudes $\Delta\sigma$ as a function of the applied temperature (see Fig. 4), only a small temperature variation within shear bands is thus anticipated. This agrees with the fact that most of the energy supplied to the system originates from the elastic loading and is partially converted into heat by a stress drop or a shear displacement. Therefore the distinct stress drops can be rather taken as a result of localized shear softening, where the shear strain rate exceeds the applied strain rate.

Relating the viscosity to the shear strain rate, however, indicates a rheological behavior which is typical of non-Newtonian shear [53,54] at high stresses and/or high strain rates, i.e. where the viscosity is not only dependent on temperature but also on strain rate. This is shown in Fig. 12b, where the sum of our results presented are shown together with results of Refs. [53,54] and those of Ref. [35] obtained in a similar manner as here from RT tests. It should be mentioned, however, that the measurements shown here and those of Ref. [35] in fact reflect the shear viscosity based on the assumption that the shear stress is approximately half the flow stress, which reflects rather a macroscopic shear stress than a microscopic one. Therefore Fig. 12b and similar plots shown in the literature need to be interpreted with care, as the viscosity measured in the homogeneous regime reflects the true viscosity over the entire volume, while the apparent viscosity estimated for the inhomogeneous regime (shear localization) does not reflect the true viscosity within the shear band, as the shear stress and thus the viscosities are overestimated. Ultimately, the above-mentioned considerations imply that the measured viscosities are a consequence of excess free volume generation during stress-assisted shearing and are not caused by temperature bursts.

4.2. Shear band nucleation and propagation

As mentioned in the previous section, SEM images strongly suggest that micrometer-sized shear displacements occur not on single atomic planes of 20 nm in thickness, but on multiple planes over time periods exceeding 1 ms. The AE measurements indicate that discrete bursts are not only observed at stress drops, i.e. when discrete macroscopic strain is formed, but AE activity is also observed in the elastic regime. This demonstrates the great sensitivity of this technique with respect to microscopic events. The recorded waveforms shown in Fig. 9c and d prove that shear banding is a complex multistage process. It is interesting to note that the stress drop duration (on average 4 ms at RT in Fig. 7) is of a different order to the time period over which high-amplitude AE is observed, which may be attributed to the activity of the source mechanism.
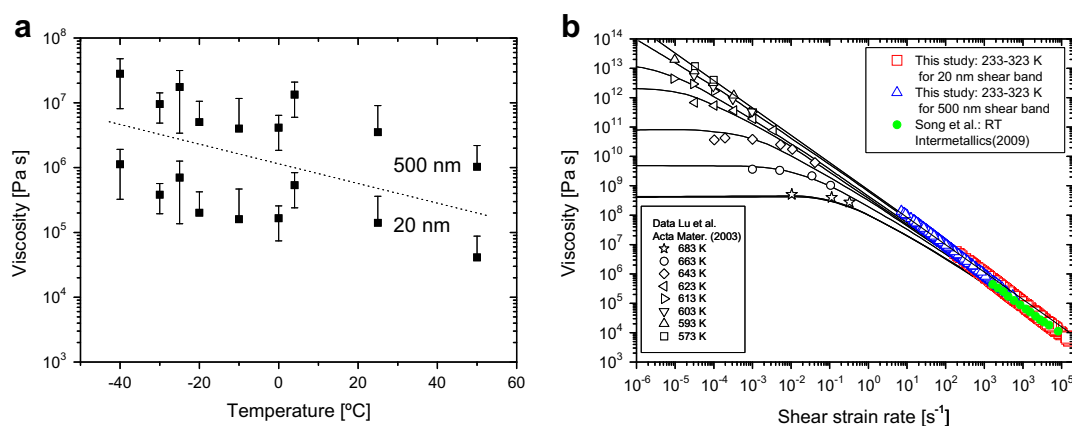
Fig. 12. (a) Apparent viscosity vs. applied temperature for a 20 nm thick shear band and for a 500 nm shear zone; (b) viscosity vs. shear strain rate including data from Lu et al. [52] measured in the homogeneous temperature range for $Zr_{41.2}Ti_{13.8}Cu_{12.5}Ni_{10}Be_{22.5}$ and data from Song et al. [35] measured at room temperature in the inhomogeneous temperature range for $Zr_{64.13}Cu_{15.75}Ni_{10.12}Al_{10}$.

Clearly, multiple, overlapping AE bursts of rise times of approximately 0.1 ms are observed (Fig. 9d) within this regime. Whether the source of AE in metallic glasses can be attributed to the collective activation of shear transformation zones and hence the nucleation of one or multiple shear bands is still the subject of ongoing work. The discrepancy in the time scales between the AE signal and the stress drop duration might then be envisaged to be due to the fact that shear band propagation giving rise to most of the macroscopic plastic strain formed does not yield any AE signal due to the highly viscous state of the shear band. It is worth emphasizing that the absence of detectable AE signals within the frequency range of 20–1000 kHz during macroscopic shear banding indicates that, at RT, shear band sliding must be a very smooth, low-viscosity process. Thus, this process, in contrast to dry stick–slip motion (where a discontinuous step-like drop in the stress during serrated flow is expected), must take place in a regime where the rheology of the material within the shear band has changed drastically from friction-dominated shear resistance to frictionless viscous flow, as also suggested by the models and the SEM images.

Furthermore, the results of Fig. 9 indicate that stress drop magnitude is governed by the effectiveness of the mechanisms stopping the shear band propagation rather than the mechanisms activating shear events. This might be related to a maximum shear band velocity, which can be sustained by the sample shortly before fracture.

The stress-assisted nucleation of an atomic shear event or shear transformation zone can, according to current literature, cause a temperature burst within a few nanoseconds, reaching temperatures several hundred or a few thousand degrees above T_g [15,26,34]. It is, however, important to note that the "quenching rate" after the discrete nanoscopic shear event has taken place can be extremely high. Therefore we believe that the temperatures during the stress drop that is associated with a shear displacement of a few micrometers and a time span of one to a few milliseconds are far lower

and not caused by this heat burst. Whether one should attribute a temperature to such a highly dynamic, low-viscosity system is probably irrelevant. However, if so, the temperature appears to be similar to T_g. This is because the decrease in viscosity may be due to stress-assisted dilatation during shear banding. In any case, however, there is no doubt that heating occurs at fracture, but then as a consequence of dissipation of a large amount of elastic energy.

5. Conclusions

Accurate compression test measurements on a Zr-based BMG were performed within a temperature range of 210–320 K, and provided new insights into the temperature dependency of serrated flow in BMGs. Results have shown that for all temperatures the shear strain rate and the stress drop magnitude increase with increasing strain, while the shear displacement increases only in the last few serrations before fracture. With decreasing temperature the stress drop magnitude decreases, while the designated time for a stress drop, which is equivalent to the time span of the mutually interrelated strain burst, increases at constant shear displacement. This allows for an accurate determination of the shear strain rate and the shear viscosity within a shear band. SEM analysis suggests that shearing in compression samples occurs simultaneously on multiple parallel stacked shear band planes, resulting in the development of a major shear zone which spreads over the entire sample dimension. The apparent viscosity measurements suggest a non-Newtonian flow behavior typical for high stresses and high strain rates.

AE signals coincide with the onset of serrations within the flow curves. The waveforms suggest a complex, multistage process of shear banding. The discrepancy in time scales of the duration of the AE signal and the stress drop might give initial indications as to the AE source mechanism not being responsible for the entire macroscopic plastic strain formed.

Acknowledgment

References

[1] Thompson PA, Robbins MO. Science 1990;250:792.
[2] Thompson PA, Robbins MO. Science 1991;253:916.
[3] Scholz CH. Nature 1998;391:37.
[4] Fialko Y, Khazan Y. J Geophys Res 2005;110:B12407.
[5] Mulford RA, Kocks UF. Acta Metall 1979;27:1125.
[6] Robinson JM, Shaw MP. Int Mater Rev 1994;39:113.
[7] Chen HS. Scripta Mater 1973;7:931.
[8] Pampillo CA. J Mater Sci 1975;10:1194.
[9] Masumoto T, Maddin M. Mater Sci Eng 1975;19:1.
[10] Kimura H, Masumoto T. Acta Metall 1983;31:231.
[11] Dalla Torre FH, Dubach A, Nelson A, Löffler JF. Mater Trans 2007;48:1774.
[12] Dalla Torre FH, Dubach A, Siegrist ME, Löffler JF. Appl Phys Lett 2006;89:091918.
[13] Dalla Torre FH, Dubach A, Schällibaum J, Löffler JF. Acta Mater 2008;56:4635.
[14] Dubach A, Dalla Torre FH, Löffler JF. Philos Mag Lett 2007;87:695.
[15] Lewandowski JJ, Greer AL. Nat Mater 2006;5:15.
[16] Schuh CA, Hufnagel TC, Ramamurty U. Acta Mater 2007;55:4067.
[17] Zhang Y, Stelmashenko NA, Barber ZH, Wang WH, Lewandowski JJ, Greer AL. J Mater Res 2007;22:419.
[18] Bruck HA, Rosakis AJ, Johnson WL. J Mater Res 1996;11:503.
[19] Gilbert CJ, Ager III JW, Schroeder V, Ritchie RO, Lloyd JP, Graham JR. Appl Phys Lett 1999;74:3809.
[20] Flores KM, Dauskardt RH. J Mater Res 1999;14:638.
[21] Hufnagel TH, Jaiao T, Li Y, Xing L-Q, Ramesh KT. J Mater Res 2002;17:1441.
[22] Yang B, Liu CT, Nieh TG, Morrison ML, Liaw PK, Buchanan RA. J Mater Res 2006;21:915.
[23] Yang B, Morrison ML, Liaw PK, Buchanan RA, Wang G, Liu CT, et al. Appl Phys Lett 2005;86:41904.
[24] Dai LH, Yan M, Liu LF, Bai YL. Appl Phys Lett 2005;87:141916.
[25] Lee MH, Sordelet DJ. Appl Phys Lett 2006;88:261902.
[26] Battezzati L, Baldissin D. Scripta Mater 2008;59:223.
[27] Wright WJ, Schwarz RB, Nix WD. Mater Sci Eng A 2001;319–321:229.
[28] Zhang Y, Greer AL. Appl Phys Lett 2006;89:071907.
[29] Wright WJ, Samale MW, Hufnagel TC, LeBlanc MM, Florando JN. Acta Mater 2009;57:4639.
[30] Pekarskaya E, Kim CP, Johnson WL. J Mater Res 2001;16:2513.
[31] Li J, Wang ZL, Hufnagel TC. Phys Rev B 2002;65:144201.
[32] Saida J, Setyawan ADH, Kato H, Inoue A. Appl Phys Lett 2005;87:151907.
[33] Song SX, Bei H, Wadsworth J, Nieh TG. Intermetallics 2008;16:813.
[34] Georgarakis K, Aljerf M, Li Y, LeMoulec A, Charlot F, Yavari AR, et al. Appl Phys Lett 2008;93:031907.
[35] Song SX, Nieh TG. Intermetallics 2009;17:762.
[36] Chen HM, Huang JC, Song SX, Nieh TG, Jang JSC. Appl Phys Lett 2009;94:141914.
[37] Spaepen F, Turnbull D. Scripta Metall 1974;8:563.
[38] Spaepen F. Acta Metall 1977;25:407.
[39] Spaepen F. Nat Mater 2006;5:8.
[40] Dubach A, Dalla Torre FH, Löffler JF. Acta Mater 2009;57:881.
[41] Han ZH, He L, Zhong MB, Hou YL. Mater Sci Eng A 2009;513–514:344.
[42] Klaumünzer D, Maaß R, Dalla Torre FH, Löffler JF. Appl Phys Lett 2010;96:061901.
[43] Passchier CW, Trouw RA. Microtectonics. Germany: Springer; 1996. p. 289.
[44] White SH, Burrows SE, Carreras J, Shaw ND, Humphreys FJ. J Struct Geol 1980;2:175.
[45] Bakai AS, Bakai SA, Mikhailovskii IM, Neklyudov IM, Stoev PI, Macht MP. JETP Lett 2002;76:218. Translated from Pis'ma v Zhurnal Éksperimental'noi i Teoreticheskoi Fiziki 2002;76:254.
[46] Vinogradov AYu, Khonik VA. Philos Mag 2004;84:2147.
[47] Stillinger FH. Science 1935;267:1935.
[48] Harmon JS, Demetriou MD, Johnson WL, Samwer K. Phys Rev Lett 2007;99:135502.
[49] Khonik VA. Solid State Phenom 2003;89:67.
[50] Waniu TA, Busch R, Masuhr A, Johnson WL. Acta Mater 1998;46:5229.
[51] Mukherjee S, Schroers J, Zhou Z, Johnson WL, Rhim WK. Acta Mater 2004;52:3689.
[52] Kawamura Y, Shibata T, Inoue A, Masumoto T. Mater Trans 1999;40:335.
[53] Lu J, Ravichandran G, Johnson WL. Acta Mater 2003;51:3429.
[54] Johnson WL, Demetriou MD, Harmon JS, Lind ML, Samwer K. MRS Bull 2007;32:644.